Available online at www.sciencedirect.com

Manufacturing Letters

Manufacturing Letters 33 (2022) 719–731

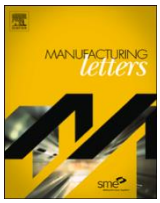

50th SME North American Manufacturing Research Conference (NAMRC 50, 2022)

Effects of surface treatments on ABS mechanical properties from fused filament fabrication

Jing-Jing Shen[a], Matthew Robert Patterson[a], Erin Marshall[a], Jake Dvorak[a], Stian Romberg[a], and Tony Schmitz[a,b*]

[a]*University of Tennessee, Knoxville, Mechanical, Aerospace, and Biomedical Engineering Department, Knoxville, Tennesse, USA*
[b]*Oak Ridge National Laboratory, Manufacturing Science Division, Oak Ridge, Tennessee, USA*

* Corresponding author. Tel.: +1-865-974-6141. *E-mail address:* tony.schmitz@utk.edu

Abstract

This paper examines the influence of surface treatments on the mechanical properties of acrylonitrile butadiene styrene (ABS) samples printed by fused filament fabrication (FFF). Prior efforts have applied brushing, painting, solvent dipping, infiltration, and vapor smoothing as post-processing surface treatments to improve the mechanical properties of FFF components. Additionally, because FFF can produce components with undesirable surface roughness, mechanical abrasion, epoxy coating, and acetone treatment may increase tensile strength by decreasing stress concentrations. Ridged surface texture may provide desirable tribological or handling properties. Based on these opportunities, this paper investigates abrasive media blasting, epoxy coating, acetone immersion, and ridged texturing surface treatments on the tensile strength and other mechanical properties of FFF ABS samples. ASTM D638-14 Type-I samples were printed, treated on all sample sides, and tested. From tensile tests, the elastic modulus, tensile strength, and fracture strain for both the untreated and treated ABS samples were calculated. For each sample, the surface finish and fracture macromorphology were observed with optical microscopy and the roughness values for the surface finish were calculated from profilometer data. Furthermore, samples were submerged in water and weighed periodically to measure mass changes due to water absorption. From surface profilometry and optical miscopy data, mechanical media blasting, epoxy coating, and immersion in all concentrations of acetone decreased surface roughness. Overall, on average, grit blasting with large beads and epoxy coating led to 2.6% and 1.2% increases in tensile strength, respectively; immersion in 40% acetone led to a 1.9% increase in tensile strength while treatment in 60% and 80% acetone decreased tensile strength by 4.9% and 1.9%, respectively. The study concludes that only grit blasting with large beads, immersion in 60% acetone, and the ridged texture significantly affected the tensile strength.

Keywords: Additive manufacturing; fused filament fabrication; ABS; material properties; surface treatment

1. Introduction

Unlike conventional fabrication techniques, such as molding, casting, and machining, additive manufacturing (AM) produces parts using a layer-by-layer approach that provides complex geometries. By printing the desired product directly from a digital design file, AM can reduce material waste and production time [1]. However, AM faces several challenges. Today, most additively manufactured polymer parts are employed as conceptual prototypes rather than functional components given their limited strength and functionality. AM can also be restricted by material properties, the speed of manufacturing, in addition to part size [2].

In fused filament fabrication (FFF), polymer materials are heated, extruded, and then sequentially deposited into layers, which then solidify due to the temperature difference between the extruder nozzle and the previously deposited material [3,4]. FFF serves as the most affordable AM method [2,4,5] and the most common polymer AM technique [6]. Despite these merits, FFF still faces challenges regarding the part's mechanical properties. The complete removal of support structures can be difficult. Anisotropy and nozzle clogging reduce effectiveness [2]. Materials produced through FFF may

have a surface roughness that does not meet application requirements [7]. Since the print head only heats material locally, the molten material can begin to cool and solidify prior to deposition, which can lead to incomplete diffusion [8]. Each deposited layer consists of cylindrical extrusion arrays, which produces void spaces between deposited material layers [8,9]. This can lead to defects, including undesirable microstructures and porosity [10], which occur through both inter-bead gaps at bead-bead interfaces as well as intra-bead voids [3]. These can function as stress concentration sites [11] that can ultimately distort the part.

Materials that can be employed in FFF are limited to thermoplastic polymers that possess a melt viscosity high enough for structural integrity, but low enough to facilitate extrusion [2]. Common thermoplastic filaments include acrylonitrile butadiene styrene (ABS), nylon, polyamides (PA) such as PA6 and PA12, polycarbonate (PC), polyether-ether-ketone (PEEK), polylactide (PLA), polypropylene (PP), and Ultem [1,3]. However, parts produced from pure thermoplastics often lack the strength or functionality of their counterparts produced through traditional injection molding or compression molding. These drawbacks are attributable to the poor interfacial bonding between adjacent beads coupled with the high void content of thermoplastic materials [3].

The layer-by-layer process of FFF can give rise to poor surface finish as a consequence of the staircase effect [12,13]. Surface treatments can help eliminate part voids, reinforce intra-material bonds [14], allow for the tuning of aesthetic properties, and protect against environmental effects [15]. Previously studied surface treatments for thermoplastic printed parts include mechanical abrasion, peel ply, plasma or laser treatments, solvent dipping, and vapor smoothing. These treatments can influence the bonding surface energy, surface roughness, and adhesion chemistry of the printed part [14–16].

By reducing or creating surface irregularities of parts fabricated through FFF, surface treatments can influence the surface roughness and uniformity of printed parts, which affect their tensile strength and ductility [12]. While mechanical media treatments physically abrade the surface, chemical treatments can dissolve the outer layers, allowing dissolved materials to fill in gaps between raster-type passes. This study examines the effects of four different surface treatments: mechanical media blasting, epoxy coating, acetone immersion, and machined ridge on the mechanical properties of ABS parts fabricated by FFF.

This work offers a unique, comprehensive comparison of three different surface treatments on the surface roughness, mechanical properties, and hygroscopic properties of ABS. The surface treatments examined differ in their mechanism of action. Grit blasting comprises a mechanical abrasion of the material surface. Epoxy coating involves the application of a layer of a distinct material atop the printed specimen. Meanwhile, acetone entails the dissolution of the printed material to arrive at a smoother finish. Even so, this study encompassed testing different bead sizes for grit blasting; specific concentrations for acetone immersion; and a facile, controllable, and replicable method for epoxy coating. In this way, we aimed to achieve a better understanding of how each of these treatments affects the surface morphology and material properties of FFF ABS.

2. Background

2.1 Surface treatments

2.1.1 Mechanical media blasting

Mechanical media blasting, also known as grit blasting (GB) or sandblasting, entails the use of an abrasive material to roughen, smooth, or shape a given surface under high pressure. Grit blasting is an effective means of tailoring the desired surface roughness of a printed part [17]. Grit blasting can either abrade the surface of a smooth object or smooth that of a rough object [18], depending on the grit size [19].

On the one hand, GB can decrease the roughness of a surface by eroding the highest peaks [19], removing excess FFF material, and reducing the stair-stepping effect [13]. In this way, GB has been found to "redistribute compressive residual stresses" [20]. Although GB can in some cases smooth the surface of a printed polymer, it can also be used to roughen a printed part [18]. Even as grit blasting wears away a surface, in this process, particles can also embed into the printed part, leading to a rougher surface with protruding particles [19,20]. In this case, by reducing the distance between peaks and valleys on the as-printed polymer surface, GB can form irregular microstructures [18].

Post-processing techniques involving media blasting have employed a variety of media, including glass beads, coal slag, and alumina nanoparticles. These media vary in their range of grit sizes and the blasting process can entail one or multiple passes [21], underscoring the complex array of factors that may affect the mechanical properties of the final printed product. Given this potential to either increase or decrease the surface roughness of printed polymers, this study examined the influence of grit blasting using two different particle sizes on the surface morphology and tensile strength of FFF ABS.

2.1.2 Epoxy coating

Epoxy resin is a thermosetting polymer commonly employed to produce adhesives, coatings, and matrix resins for composite materials. Several experiments have examined the use of epoxy to repair fractured samples of FFF ABS-epoxy composites, [22,23] but comprehensive studies investigating the effects of epoxy coatings on samples manufactured specifically using FFF have yet to be conducted. As a surface treatment, epoxy can improve mechanical properties such as tensile strength and elastic modulus, as well as thermal and chemical resistance [24]. Some epoxies have favorable material properties compared to ABS [25-27]. Research has shown that epoxy can readily fill in pores of materials [28]. Specific to its applications for ABS, one study found that an epoxy resin-infilled lattice structure of ABS demonstrated a yield strength of 41.9 MPa and ultimate strength of 85.72 MPa, both of which were superior to those of a neat ABS sample (31.19 MPa and 50.96 MPa, respectively) [29]. Epoxy does pose several challenges, however, including its brittleness, low fracture strength, and low impact strength [24]. Epoxy-ABS adhesion is known to be low, but this can be improved with cold plasma treatment [30]. Moreover, bulk epoxy is typically a more expensive material than bulk ABS; therefore, a composite-based approach with a high weight percentage of

epoxy will significantly increase the cost of manufacturing components [31,32].

Various methods have been explored for applying epoxy coatings to materials. A desired coating of epoxy should be uniform [28], which requires careful consideration of infiltration time in addition to mitigating leakage and air bubble formation [14]. Alternatively, an epoxy coating can be applied as an aerosolized spray, which costs less [33]. Another technique is vacuum infiltration, in which samples are immersed in a sealant of epoxy and then subjected to a vacuum environment. Although this method requires large amounts of infiltrant, it can mitigate the formation of air bubbles [28] and allows for a thorough penetration of epoxy into the polymer substrate. Finally, a simpler alternative to vacuum infiltration is brushing epoxy onto the sample directly, which is often employed when the former is not feasible.

Epoxy coatings must be cured after being applied. Curing permits the epoxy to facilitate both crosslinking and chemical reactions at the interface of the epoxy and the substrate, which can assist in the formation of strong bonds between and with the printed beads [11]. Importantly, in this process, a room temperature cure can be helpful to mitigate any thermal distortions.

Theoretically, a thin layer of epoxy coating can smooth stress concentration regions by decreasing surface roughness and the diffusion of epoxy into voids present in the internal structure of the part, thereby helping strengthen the component [34]. It is not known, however, how deep the epoxy will diffuse into the substrate, or how the base material strain affects the epoxy adhesion.

2.1.3 Acetone immersion

Acetone is commonly used for postprocessing AM parts, specifically for polylactic acid (PLA) and ABS. Upon application, acetone dissolves the top layer of ABS and then diffuses, allowing the surface plastic to resolidify with a smoother surface [35,36]. Acetone can be applied using immersion, hot vapor, or cold vapor treatments. Immersion refers to the process of fully submerging a sample in an acetone solution, whereas vapor treatments use either room temperature vapors (cold treatment) or heated acetone that evaporates into hot vapor. Of these methods, immersion offers the most rapid yet consistent results. Hot vapor treatments are rapid but difficult to control [35], and cold vapor treatments take more time than immersion, reducing its effectiveness for mass production.

Unlike mechanical abrasion or epoxy brushing, which both depend upon manual consistency, acetone immersion is relatively uniform in its application. However, prolonged exposure to high concentrations of acetone can also affect the part geometry and make samples unsuitable for further use [37]. For acetone to be most effective, it is necessary to determine the ideal conditions to smooth the surface texture without eroding a significant portion of the samples. Furthermore, while this treatment has been shown to increase ductility and decrease surface roughness, concomitant decreases in tensile strength have also been observed [38].

Previous studies have exposed ABS specimens to an acetone vapor solvent and found decreases in surface roughness, increased strain to failure, and negligible impact on the mechanical properties of ABS [39, 40]. In contrast to hot or cold vapor treatment—methods of applying acetone that have been extensively examined—immersion in acetone is a fast process that can be conducted at room temperature. Nonetheless, the strong dissolution capabilities of acetone carry risks of damaging the part surface, rendering the solvent difficult to control [41]. To optimally balance consistent, controlled application of acetone with minimal deterioration of the material, this study sought to thoroughly explore the effect of different concentrations of acetone solvent via a short immersion time on the properties of ABS.

2.1.4 Ridged texture

Raised ridge textures have been shown to reduce wear in components subjected to abrasive particles [42]. Aziz *et al.* found that ribbed pattern size plays an important role in the wear of a 3D printed component during pin-on-disc testing [43]. Ribbed textures also create a unique feel in hand-held components and can be used to aid grip in hand tools, medical devices, and robotics [44-46]. Research has been conducted on how ridges can improve ergonomics in 3D printed components [47], but the effect of ridged geometry on the material properties of 3D printed ABS has yet to be explored. This paper explores two processes for creating ribbed geometry: printing the ribbed surface directly onto a specimen and the creation of ridges by machining away excess material.

2.2 Material properties: tensile strength and surface morphology

Tensile testing facilitates the study of the "macroscopic mechanical signature" of printed parts, which can identify the strength of materials in addition to how they fail [48]. Characterizing mechanical properties, including elastic or Young's modulus (YM), tensile strength (TS), and fracture strain, is common. In addition to quantifying mechanical properties, assessing surface morphology through surface profilometry and micrography can locate voids formed during the FFF process. These voids are the gaps that form between beads as the beads of material are printed, leading to the creation of stress concentration points that may explain tensile failures [6].

2.3 Humidity absorption and mass change

Beyond the properties of printed FFF ABS, it is also important to note that since polymer matrices have the capacity to absorb water, the material must be dried before it is used in printing to mitigate the formation of detrimental bubbles and pores [48]. Nonetheless, the FFF process can still create voids at bead-to-bead interfaces, which can make projects prone to absorbing water from the environment. The percentage of humidity in the atmosphere and following permeation into the material itself can therefore affect both the quality of the surface finish and the dimensional accuracy of parts [13]. Upon absorption of moisture, the material can become degraded, which will then increase the variation in printed products and possibly contribute to a decrease in tensile strength. ABS possesses hygroscopic tendencies, in which the polymer can absorb or adsorb water present in the surrounding environment [49].

According to literature, polyurethane and acrylic coatings on FFF manufactured samples can decrease water absorption, while leaving the tensile strength relatively unaffected [36]. Neat epoxy and epoxy composites have been observed to limit water absorption compared to other materials [50,51], but it is not known if an epoxy coating will achieve similar results. Therefore, in this study, the effects of surface treatments on the water absorption of the printed products were also examined through repeated mass measurements to track the moisture absorption of the treated versus neat ABS samples.

3. Materials and methods

The experimental methodology is outlined in Fig. 1. For this study, the ASTM D-638 Type 1 sample geometry was used. Stratasys Insight software was used to create an alternating 45 degree raster pattern with a solid infill. A layer height of 0.254 mm was chosen. Samples were printed on a Stratasys Fortus 250mc FFF printer [52] using Stratasys Blue ABSplus-P430 filament from new stock [53]. An XY (flat) layer orientation was used to arrange 10 samples onto the print plate. For each surface treatment subgroup (including both sizes of glass beads for mechanical media blasting; epoxy coating; and all concentrations of acetone), a total of 10 samples were printed, assessed, and treated. After printing, each sample was measured, massed, and its surfaces were studied with microscopy and stylus profilometry. Then, surface treatments were applied to the top, bottom, sidewall, and edges of each sample. Next, sample surfaces were characterized once more. Lastly, tensile tests were completed using an MTS Criterion Model 45 universal testing machine (UTM); see Fig. 2 [54].

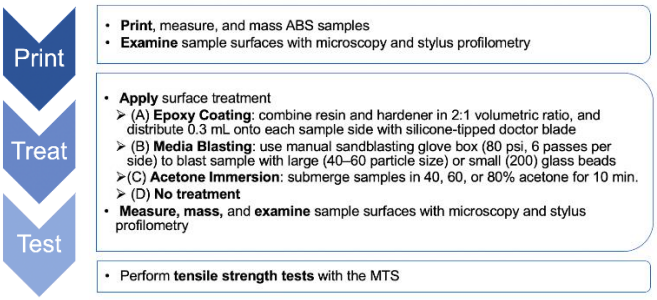

Fig. 1. The experimental procedure.

Fig. 2. A tensile test using the UTM.

According to the manufacturer specifications from Stratasys for the ABS filament, the tensile strength of the material is 33 MPa, YM is 2.2 GPa, and the fracture strain is 6% [53]. In total, 20 untreated test specimens were created and tested to use as a baseline for the treated specimens. Prior to each tensile test, the surface topography/morphology was assessed using microscopy. First, a Mitutoyo Surftest SJ-210 stylus profilometer [55] was used to obtain a measurement for the surface roughness of the sample for all sample types except the ridged samples. For the ridged samples, surface profiles were captured using a Keyence VR 5100 3D measurement system.

For each dogbone test specimen, four locations were measured to determine average roughness values or R_a [13]. The ISO 1997 standard was used in conjunction with Gaussian filtering with a 0.25 mm cut-off and a wavelength, λ_s, of 2.5 µm. Given that stylus profilometers cannot fully enter every pore on the surface of the sample [18], optical microscopy was also employed to obtain more data regarding the topography of both the sample surface and fracture site. A VHX 5000 Keyence digital microscope was used to examine multiple locations on the surface of each dogbone sample.

3.1 Surface treatments of samples

3.1.1 Mechanical media blasting

To study how mechanical media blasting affects the surface properties and tensile strength of FFF ABS, the surfaces of printed dogbone samples were subject to media blasting with either large glass beads (40 to 60 grit, 254 µm to 365 µm diameter) or small glass beads (200 grit, 84 µm diameter) obtained from McMaster-Carr. A total of six passes per side were completed in a Trinco Dry Blast Cabinet (Model 3G7BP) manual sandblasting glove box. The media were propelled by compressed air from an air-pressure gun at a pressure of 80 psi, with the nozzle of the device at a distance of approximately 10 cm from the sample surface.

Following the blasting, a WypAll shop cloth was used to remove loose particles from the samples, which were then permitted to air dry. Samples were again massed and examined using light microscopy as well as stylus profilometry. Tensile tests were performed using the MTS.

3.1.2 Epoxy coating

The effects of epoxy coating on the mechanical properties of FFF ABS were also explored. For this study, Smooth-On XTC-3D High-Performance epoxy coating was chosen given its commercial availability and specific intended application for FFF manufactured components. Epoxy resin and hardener were combined in a 2:1 volumetric ratio and mixed for one minute, per manufacturer specifications. Afterward, 0.3 mL of the epoxy mixture was loaded into a syringe and deposited on one side of the printed dogbone samples using a silicone-tipped doctor blade; see Fig. 3. After two hours of curing at room temperature, samples were flipped over and the coating procedure was repeated for the remaining side, as well as for the sidewall and edges of the sample.

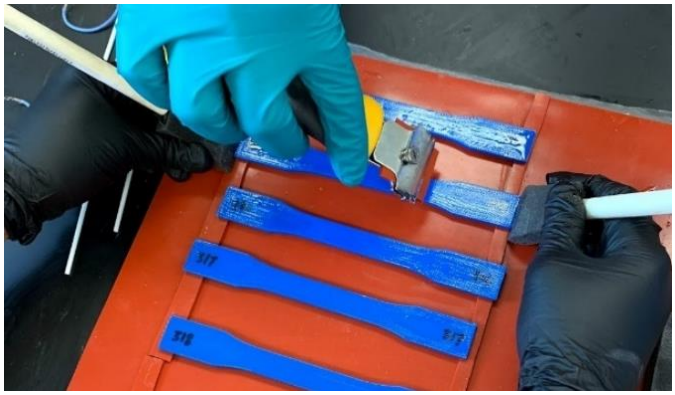

Fig. 3. Applying the epoxy coating to a specimen.

The only material property provided by the epoxy manufacturer was a Shore hardness of 80D. Therefore, to obtain additional mechanical properties of the neat epoxy, the epoxy resin was cast into a silicone mold and ASTM D638-14 Type I samples were prepared using a water jet cutter.

3.1.3 Acetone immersion

To investigate how acetone submersion affects the tensile properties of ABS, test samples were immersed in varying concentrations of liquid acetone (obtained from Sunnyside). Dogbone samples were fully submerged in either a 40%, 60%, or 80% by volume acetone solution, with 15 samples assigned to each concentration. For each treatment group, a batch of five samples was immersed in the corresponding solution for a duration of 10 minutes, and the same solution was used for all three batches.

After immersion, the 40% and 60% acetone samples were removed from the solution, patted dry with paper towels, and placed upright along their long edge to dry overnight and evaporate any remaining acetone or water. To prevent the "bowing" tendency previously observed with the 80% acetone samples, these specimens were laid horizontally on a silicone mat to dry.

Once the samples were dried, they were massed again to record any change due to residual moisture, and the treated surfaces were again examined. Finally, all treated samples were tensile tested.

3.1.4 Ridged texture

To create the printed ridged specimen, the dogbone specimen file was modified by adding ridges on the specimen surface at a 45 degree angle; see Fig. 4. Each ridge had a height of two layers, 0.53 mm ± 0.05 mm, a width of 0.96 mm ± 0.07 mm, and a spacing of 1.1 mm ± 0.05 mm. The same print parameters were used to slice the model.

To create the CNC milled samples, 11 specimens were printed with the same parameters as the original samples, except that the specimen thickness was set to 4.2 mm. The excess material was removed with a Haas-4VF CNC milling machine. The specimens were held in place with aluminum soft jaws during machining. First, the top and bottom surfaces were faced using a 19.05 mm diameter carbide three-flute flat end mill with a TiCN coating manufactured by HTC Tool [56], and 0.1 mm was removed from each surface. Approximately one-half of a single print layer was removed from each side to minimize the effect of bead geometry on surface finish. A spindle speed of 3621 rpm and feed per tooth of 0.02 mm were selected to achieve an adequate surface finish. To create the ridge geometry, a two-flute 1.19 mm diameter flat endmill was used with an axial depth of 0.5 mm, along with a spindle speed of 7500 rpm and a feed per tooth of 0.08 mm. A final facing pass at the same height as the first pass was used to remove any burrs.

3.1.5 Structured light scanning

A GOM ATOS Core 200 structured light scanner was used to create a 3D representation of the ridged samples. The scanner projected a two-dimensional fringed pattern of blue light onto the scanned component, and light reflected off the component surface was observed by two cameras. The geometry was calculated by observing the spacing and warping of the projected line pattern. Fiducial markers were placed on the sample prior to scanning and used to provide reference data to allow multiple scan angles to be stitched together into a single point cloud. The point cloud was then converted to a polygonized mesh [57]. GOM specified the point spacing for the Core 200 to be 0.08 mm at a 250 mm scanning distance [58]. However, scanning uncertainty was difficult to quantify due to errors introduced by the optical system, reflectivity of the scanned object, and foreshortening of scanned object geometry [59].

Fiducial marking stickers were placed on each side of the samples before scanning. After capturing scans from multiple points of view, the resulting point clouds were converted to a mesh using a post-processing setting of "More Details" and a post-process factor of 1.00 in GOM Inspect software. To confirm the accuracy of each mesh, digital calipers were used to physically measure the ridge and valley heights of each physical sample, and analogous measurements were taken using simulated calipers in software. Samples whose scan measurements did not fall within $\pm$ 0.08 mm of the physical measurements were not used for testing.

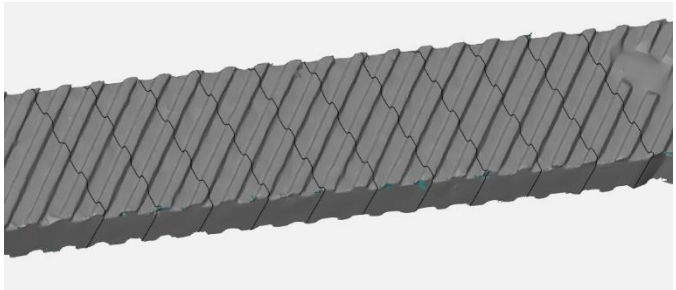

Fig. 4. A scanned specimen with cross-section samples used to calculate the average gauge length area.

Scans produced without using any scanning spray consistently produced undersized mesh geometry, especially with respect to sample thickness; see Fig. 5 for an example measurement. It was assumed that the reflectivity and blue sample color were the primary sources of these errors. Therefore, the samples were sprayed with AESUB scanning spray to reduce the surface reflectivity. Some samples contained curvature which introduced errors when multiple scans were stitched together. Therefore, only the five flattest samples of each process were scanned and tested.

To quantify the uncertainty in the scanning process, a single ridged sample was scanned six times using the previously described methodology. The sample was wiped clean after each scan, and the spray was reapplied. The average cross-sectional area of 11 regions in the gauge length was calculated using the GOM Inspect software. The standard deviation of the cross-sectional area was calculated to be 1.8%, a large variation possibly attributable to several reasons. First, the scan results were very sensitive to the amount of spray used during the sample preparation. Hand spraying the samples produced uneven coverage. Additionally, the spray began to sublimate during scanning and needed to be reapplied on some surfaces. These findings create uncertainty in the measurements that were calculated using the cross-sectional area, including YM and TS. However, the fracture strain calculations were not affected. More research is needed using different scanning methodologies to provide more accurate results for the material properties that are dependent on cross-sectional area.

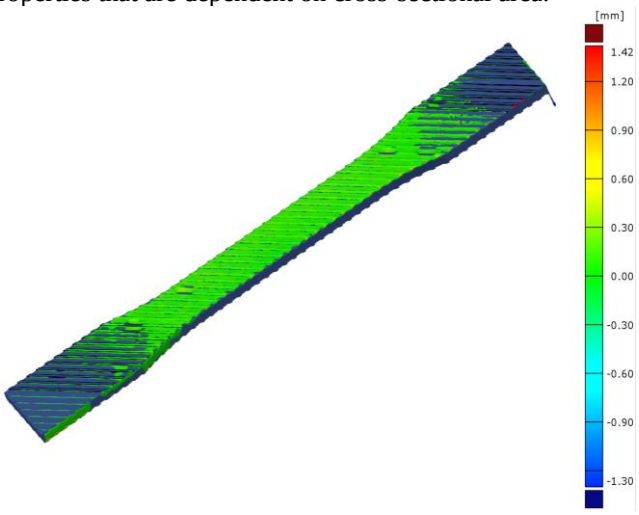

Fig. 5. A machined ridged specimen with a difference map to the CAD file.

3.2 Characterization

Following each surface treatment, samples were measured once more, and the morphology of their surfaces was examined again using microscopy and stylus profilometry. Mass measurements were also completed, and three samples from each treatment group were set aside for water immersion testing.

To complete the tensile testing of the neat and treated ABS samples, an MTS Criterion Model 45 universal testing machine with a 100 kN load cell was employed. Each test specimen was clamped at both ends and pulled at a strain rate of 5 mm/min until failure; see Fig. 2. Two pieces of reflective tape were applied at the boundary of the gauge length, and an MTS laser extensometer [60] with a 50 mm gauge length was used to measure the change in length.

3.3 Water immersion tests

To assess the hygroscopic tendencies of the treated versus untreated ABS, water absorption tests were conducted. From each treatment group, three sample specimens were set aside for water absorption. Before water immersion, each sample was massed following printing (before treatment) and once more after treatment. Samples were entirely immersed in a graduated cylinder filled with water for eight hours. At every hour during this period, samples were removed from the water, massed, and then returned to the water. These mass change measurements were used to calculate the absolute and percent mass change for each sample. To note, as each of the three surface treatments was applied to the top and bottom faces of each sample, along with their sidewalls and edges, water immersion test results were attributable to their respective surface treatments.

4. Results and Discussion

4.1 Surface morphology and profiles

Following surface treatment, each sample surface was characterized using light microscopy and surface profilometry. Additionally, the fracture macromorphology and tensile deformation were examined after tensile testing. Surface profiles for samples from every treatment group are shown in Figs. 6 and 7. All R_a values are listed in Table 1.

Surface profilometry of the neat ABS samples yielded R_a values of 2.4 µm and 4.8 µm for the top and bottom sides, respectively. The bottom surfaces of the specimens, which contacted the print bed during fabrication, tended to be rougher than the top surfaces. These R_a values served as comparison baselines for those of other surface treatments. For the untreated ABS samples, optical microscopy (Fig. 11a) revealed noticeable voids within the samples.

Samples treated with media blasting of small beads showed increased surface roughness in the top surfaces, while a decrease in roughness was observed for the bottom surfaces; see Fig 7. Optical microscopy for samples from both treatment groups showed that beads of both sizes led to noticeable changes at the voids of the ABS. While small beads tended to remain lodged in the gaps, large beads appeared to discolor the surface with pockmarks without becoming stuck in the voids themselves (Figure 11c).

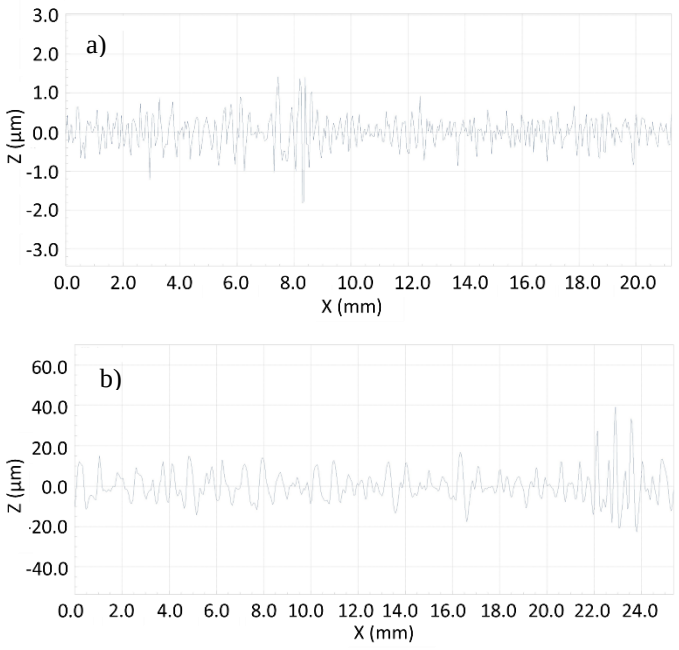

Fig. 6. Surface profiles for: a) machined ridged sample and b) printed ridged sample.

Table 1. Pre-treatment and post-treatment R_a values.

Treatment	Top R_a (µm)		Bottom R_a (µm)	
	Pre	Post	Pre	Post
Neat ABS	2.4	-	4.8	-
Grit blasted – small beads	2.6	2.8	5.0	0.03
Grit blasted – large beads	2.2	1.2	5.0	2.1
Epoxy – neat	0.04	-	0.21	-
Epoxy – brushed	2.2	0.04	6.3	1.2
Acetone – 40%	2.1	2.1	4.0	3.8
Acetone – 60%	3.6	0.76	5.0	2.2
Acetone – 80%	3.2	0.01	5.0	0.08
Ridges – machined	2.3	0.30	4.4	1.3
Ridges – printed	5.5	-	2.9	-

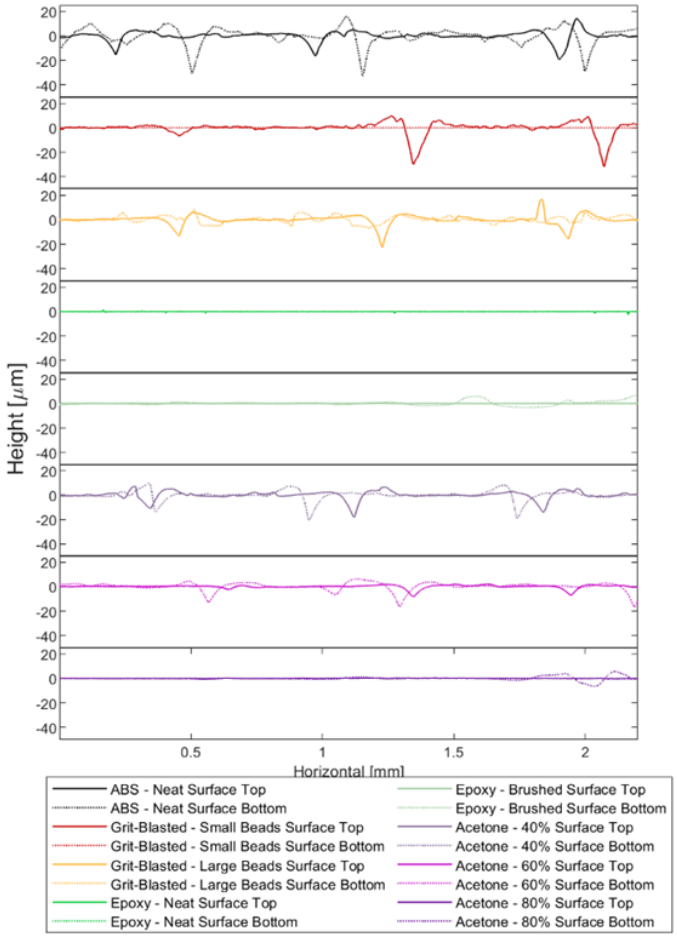

Fig. 7. Surface profiles for all sample types excluding the ridged geometry (shown in Fig. 6).

Following coating with epoxy, the mean R_a values for both the top and bottom surfaces of the epoxy-coated ABS decreased compared to those of neat ABS. Notably, the neat epoxy samples, which exhibited especially small R_a values (0.043 µm and 0.211 µm for the top and bottom sides of the specimens, respectively) were also observed to have smooth surfaces overall. Even so, small air bubbles speckled the surface (Fig. 11d). Optical microscopy also confirmed that the application of the epoxy coating to the ABS was able to smooth out both sides of the dogbone samples, as several voids throughout the samples were noticeably filled; see Fig. 8.

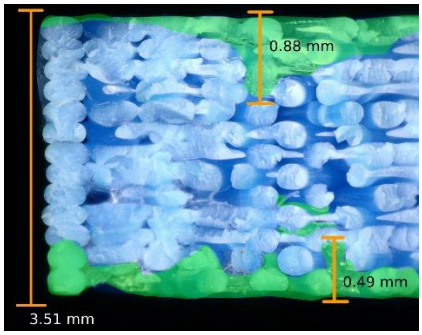

Fig. 8. The relative penetration of epoxy into the ABS substrate (green coloration added for emphasis).

Immersion in acetone of any concentration led to decreases in surface roughness for both the top and bottom surfaces of ABS, suggesting that the solution was able to smooth out some of the ABS. The decrease in R_a values was greater in samples submerged in higher concentrations of acetone; see Table 1. Similar results were also observed in the optical microscopy images of the samples, in which the smoothness and "glossiness" of the sample surfaces appeared to increase with increases in acetone solution concentration; see Fig. 9.

Ridged samples created using machining demonstrated a dramatic increase in R_a with a value of 0.3 µm and 1.2 µm in the top and bottom surfaces. The printed ridged samples possessed similar roughness to the neat ABS samples, as expected.

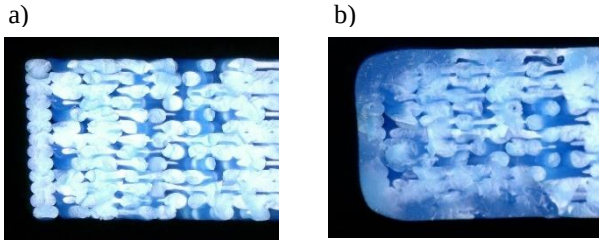

Fig 9. Specimens treated with: a) 40% and b) 80% acetone solution.

4.2 Data analysis methodology

Engineering stress-strain curves (Fig. 10) were generated in MATLAB using the force data from the MTS crosshead and length change from the laser extensometer. In order to calculate YM for the samples, points 20-90 of the stress-strain curve were fit to a first-degree polynomial with an intercept of 0 MPa. See Eqs. 1-3,

$$\sigma = \frac{F}{A} \tag{1}$$

$$\epsilon = \left|\frac{l_0 - l_i}{l_0}\right| \tag{2}$$

$$YM \approx (\sigma/\epsilon)_{linear\ region} \tag{3}$$

where σ is stress, F is the force measured by the load cell, A is the cross-sectional area at the gauge section for the given sample, ϵ is the strain, l_0 the original gauge length, and l_i the gauge length at a specific data point as measured by the laser extensometer.

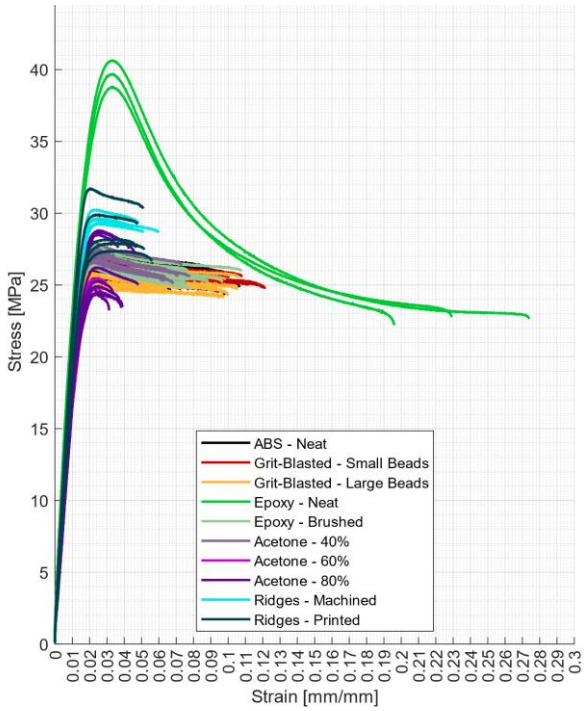

Fig. 10. Stress-strain curves for all specimen types.

Points 1-20 of the stress-strain data were excluded because slack in the mechanical components of the MTS system can create inaccurate results at the beginning of each test. For the epoxy-coated samples, two linear regions were identified. The YM for the second linear region was calculated using the same method as the first region and points 100-160 of the stress-strain curves; see Fig. 12. The maximum stress value was identified as the tensile strength

F-tests for all sample types were calculated in MATLAB in order to identify if the variance of each mechanical property was statistically different from that of the control group. Depending on the results of the F-tests, pooled t-tests or t*-tests were completed to identify if each treatment type was statistically different from the control group for each material property. The results are provided in Table 2.

4.3 Surface microscopy results

The effects of the surface treatments on the sample mechanical properties are described in the following sections. In numerous cases, including the use of mechanical media blasting, epoxy coating, and acetone immersion, the application of the surface treatment was observed to lead to a visible "joining" of printed beads [12] that were initially separated by voids. This process may help explain the surface treatments effects on the YM, TS, and fracture strain. Nonetheless, in many cases, observation of samples post-testing revealed that voids were still present, suggesting that leakage, air bubble formation, and leftover stress concentration sites contributed to failure.

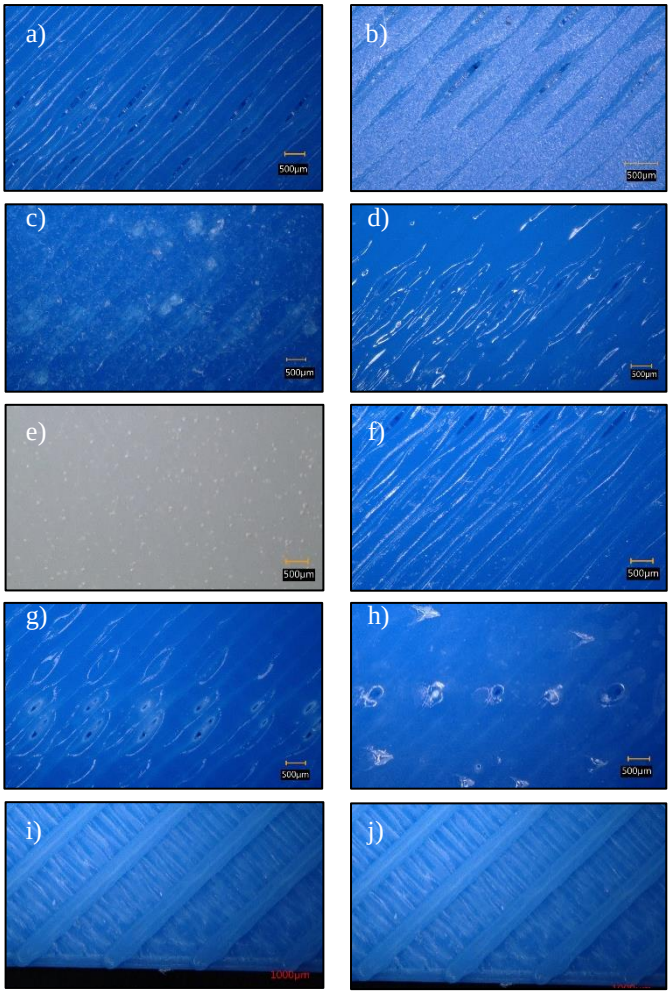

Fig. 11. Microscopy images for: a) neat ABS, b) grit blasted, small beads, c) grit blasted, large beads, d) epoxy, brushed, e) neat epoxy, f) 40% acetone, g) 60% acetone, h) 80% acetone, i) ridges, printed, j), ridges, machined.

4.3.1 Mechanical media blasting

Previous research has reported mixed results from grit blasting, which can either decrease surface roughness through erosion or increase roughness through embedding particles into the surface, based on the substrate material and bead characteristics [18, 19, 20]. Indeed, in this study, different effects on ABS were observed depending on the size of glass beads used. Overall, grit blasting the ABS samples with either small or large beads led to the surface textures of both sides of the sample becoming more like each other. Media blasting with small beads did not have any significant effect on YM, although a significant increase in fracture strain was noted. Small beads were visibly embedded in the voids of the sample surface, demonstrating the ability of these particles to fill in some ABS voids. Media blasting with large beads did not lead to any significant impacts on YM or fracture strain; rather, slight decreases in tensile strength were observed. Given the larger size, these larger beads did not embed in sample voids but instead tended to discolor the ABS surface with pockmarks.

4.3.2 Epoxy coating

Neat epoxy demonstrated a significantly higher YM and TS, as well as smoother surface morphology compared to neat

ABS. Even though this underscores the promise of neat epoxy, which can also be a 3D-printed material, the printing process can be complicated and expensive. Casting limits the geometry that can be produced, which can also pose a challenge to utilizing neat epoxy as a material in additive manufacturing.

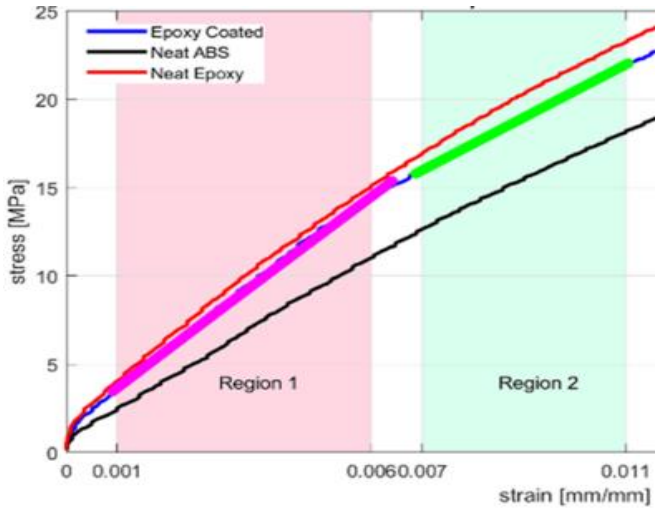

Fig. 12. Comparison of elastic moduli between untreated ABS, neat epoxy, and epoxy-coated samples. Two distinct elastic moduli are visible for the epoxy-coated samples.

For the brushed epoxy ABS samples, it was noted that YM of the epoxy-coated samples, which consist of ABS coated with epoxy resin, was between that of neat epoxy and neat ABS, confirming expectations for the composite material. Additionally, epoxy-coated samples yielded a higher YM compared to neat ABS (11.1% increase), together with a smoother surface texture than neat ABS. The superior YM of the epoxy-coated samples may be a consequence of epoxy infiltration, which has been reported to strengthen interlayer bonding [30]. The penetration of epoxy was uneven across the samples. At its maximum, epoxy penetration was approximately 80% per side with a significantly lower average penetration; see Fig 8. Penetration was higher in regions of the sample with high surface porosity.

Even though the brushed epoxy samples had a higher YM, the tensile strength was not significantly different. It is likely that the epoxy began to delaminate from the ABS at a relatively low strain, leading the samples to behave more like neat ABS samples in terms of tensile strength. Figure 13 shows a visible change in YM for region 2 that is within 0.5% of the neat ABS YM at around 0.6% strain, suggesting the epoxy and ABS have delaminated.

4.3.3 Acetone immersion

Tensile test results from the samples immersed in acetone reveal results that differ depending on the concentration of acetone used. Treatment with 40% acetone did not have any significant effect on YM, yield strength, or surface morphology, but a decrease in fracture strain was noted. On the other hand, immersion in 60% acetone contributed to a smoother surface texture, decrease in YM, and a significant 67.6% reduction in fracture strain (and, thus, a brittle fracture mode). Finally, submersion in 80% acetone led to the most prominent smoothing of the sample surface, a 54.4% decrease in fracture strain (brittle fracture), and warping of the sample into a curved geometry. Hence, the smoother surface observed for samples following immersion in 60% and 80% acetone is consistent with findings from previous literature noting that high concentrations of acetone (around 90%) reduce surface roughness and tensile strength [12, 38].

4.3.4 Ridged texture

Both types of ridged samples, printed and machined, showed significant changes in fracture strain and TS but no other properties. Fracture strain decreased by 40.4% and 39.3% in the machined and printed ridged samples, respectively. Tensile strength increased 11.4% and 9.0% in machined and printed ridged samples, respectively, with a higher variance for the printed ridges. Breaks outside of the gauge length were more common with the printed ridge samples than any other sample type. The observed fracture morphology followed the orientation of the ridges for the printed ridged samples. The early failure of the ridged samples could be due to an increase in stress concentration in the ridge geometry. Stress induced during the machining process likely did not affect the fracture strain, as both the printed and machined ridged samples fractured at similar strain levels.

4.4 Water absorption tests

The percent mass change of the immersed samples (relative to the as-printed specimens) due to the surface treatment and follow-on water absorption, are displayed in Figs. 13 and 14. The average percent mass change for water-immersed samples from each treatment group is displayed in Fig. 13. Error bars identify the 95% confidence intervals, and red stars denote which treatments held statistical significance in comparison to neat ABS. In Fig. 14, the first data point, corresponding to the "As-Printed" x-axis label, refers to the neat ABS sample before it was subject to a surface treatment condition. The second data point, designated by the "As-Treated" label, refers to the time point following the application of the treatment. Time 0:00 references the time following treatment but prior to submersion in water, and subsequent values record the percent mass change of the sample at one-hour intervals. The slopes of each line segment display the approximate percent mass increase or decrease relative to the mass recorded at the previous time point.

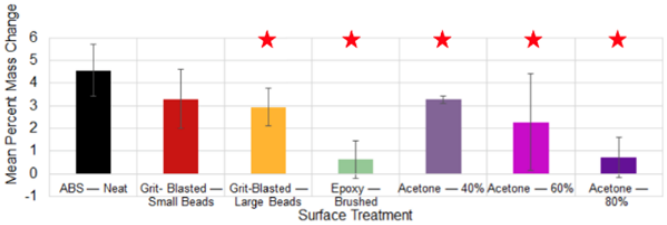

Fig. 13. Mean percent mass change due to both surface treatment and water absorption, with 95% confidence intervals. Stars indicate treatments with statistical significance.

Table 2. Material properties of all sample types, bold font indicates a statistical significance from baseline.

	Young's modulus (MPa)	Tensile strength (MPa)	Fracture strain (%)
Neat ABS (value ± std. dev)	2183 ± 83	26.6 ± 0.7	8.34 ± 0.01
Grit blasted – small beads	2232 (2.2% increase)	26.5 (0.4% decrease)	**10.2 (22% increase)**
Grit blasted – large beads	2188 (0.2% decrease)	**25.9 (2.6% decrease)**	8.8 (6.0% increase)
Epoxy – neat	**2843 (30.2% increase)**	**39.7 (49.2% increase)**	**23.3 (180.7% increase)**
Epoxy – brushed	**2426 (11.1% increase)**	26.9 (1.2% increase)	8.1 (2.4% decrease)
Acetone – 40%	2224 (1.9% increase)	27.1 (1.9% increase	**6.4 (23.2% decrease)**
Acetone – 60%	**2011 (7.9% decrease)**	**25.3 (4.9% decrease)**	**2.7 (67.6% decrease)**
Acetone – 80%	**2020 (7.5% decrease**	26.1 (1.9% decrease)	**3.8 (54.4% decrease)**
Ridges – machined	2261 (3.6 % increase)	**29.6 (11.4% increase)**	**4.99 (40.4 % decrease)**
Ridges – printed	2267 (3.8% increase)	**29.1 (9.0 % increase)**	**5.1 (39.3% decrease)**

From these data, brushed epoxy showed the best performance in terms of reducing mass change due to water absorption. Meanwhile, immersion in 80% acetone provided comparable results. Even so, submersion in 80% acetone weakened the ABS component, as evidenced by the bowing of the sample. In general, all surface treatments, except for grit blasting with small beads, were able to significantly ($\alpha = 0.05$) reduce percent mass change due to hygroscopic absorption, relative to neat ABS.

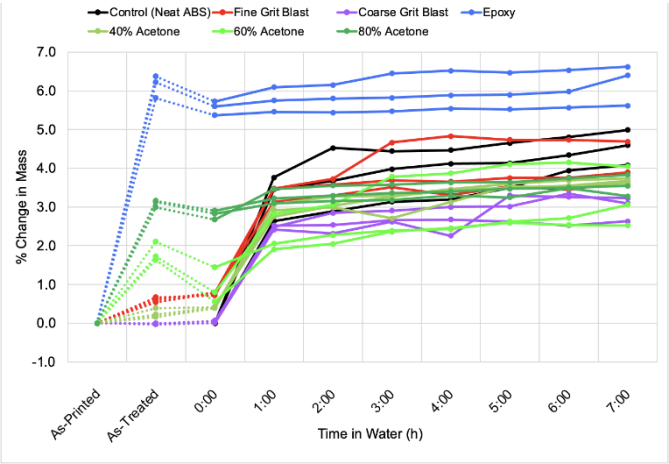

Fig. 14. Percent mass change due to both surface treatment and water absorption.

5. Conclusions

The surface treatments examined in this study—excluding grit blasting with large beads, immersion in 60% acetone, and both types of ridge geometry—did not exhibit significant effects on the ABS tensile strength. However, grit blasting with small beads was observed to increase fracture strain compared to neat ABS, even as acetone immersion in either 40%, 60%, or 80% solution led to more brittle fracture modes. The small gain in tensile strength (9% to 11%) was offset by a large decrease in fracture strain (40%) in the ridged samples. Epoxy brush coating contributed to notable increases in Young's modulus, alongside minimizing moisture uptake. Overall, considering the insignificant influence of most of the surface treatments studied on Young's modulus or tensile strength of ABS, this study concludes that these surface modifications can instead be customized to tune the desired mechanical properties**,** ranging from improved tensile strength or fracture strain to enhanced moisture resistance. Through a comprehensive investigation of three distinct types of surface treatments together, this paper uniquely offers an understanding of their effects on the tensile and mechanical properties, surface roughness, and humidity absorption properties of FFF ABS. In sum, our research findings enable a convenient and novel side-by-side comparison for FFF ABS treated using three different approaches.

So far, a wide range of surface treatments, beyond those in this study, have emerged as promising ways to improve mechanical properties, from chemical surface treatments with nanoparticles [2] and adhesion promoters [48] to annealing and flame and plasma treatments [61]. Besides novel surface modifications, progress remains to be made in the study of the underlying base materials, including polymers reinforced with carbon fibers [2,9] and other carbon-based materials [3] to thermoplastic polymers besides ABS, including polylactic acid (PLA), polyamide (PA), and polycarbonate (PC) [2]. Considering the range of possible materials and their uses, the continued exploration of surface treatments has the potential to advance the understanding of 3D printed materials and their applications in engineering, medicine, and beyond.

Acknowledgements

This work was supported by the DOE Office of Energy Efficiency And Renewable Energy (EERE), Advanced Manufacturing Office (AMO), under contract DE-AC05-00OR22725. The US government retains and the publisher, by accepting the article for publication, acknowledges that the US government retains a nonexclusive, paid-up, irrevocable, worldwide license to publish or reproduce the published form of this manuscript, or allow others to do so, for US government purposes. DOE will provide public access to these results of federally sponsored research in accordance with the DOE Public Access Plan (http://energy.gov/downloads/doe-public-access-plan).

References

[1] Shanmugam V, Rajendran DJJ, Babu K, Rajendran S, Veerasimman A, Marimuthu U, et al. The mechanical testing and performance analysis of polymer-fibre composites prepared through the additive manufacturing. Polym Test 2021;93:106925–42.

[2] Wang X, Jiang M, Zhou Z, Gou J, Hui D. 3D printing of polymer matrix composites: A review and prospective. Compos Part B Eng 2017;110:442–58.

[3] Papon EA, Haque A, Spear SK. Effects of functionalization and annealing in enhancing the interfacial bonding and mechanical properties of 3D printed fiber-reinforced composites. Mater Today Commun 2020;25:101365–76.

[4] Cardoso RM, Kalinke C, Rocha RG, dos Santos PL, Rocha DP, Oliveira PR, et al. Additive-manufactured (3D-printed)

electrochemical sensors: A critical review. Anal Chim Acta 2020;1118:73–91.
[5] Pandelidi C, Bateman S, Piegert S, Hoehner R, Kelbassa I, Brandt M. The technology of continuous fibre-reinforced polymers: a review on extrusion additive manufacturing methods. Int J Adv Manuf Technol 2021;113:3057–77.
[6] Tekinalp HL, Kunc V, Velez-Garcia GM, Duty CE, Love LJ, Naskar AK, et al. Highly oriented carbon fiber–polymer composites via additive manufacturing. Compos Sci Technol 2014;105:144–50.
[7] Rojas-Nastrucci EA, Weller T, Aida VL, Cai F, Papapolymerou J. A study on 3D-printed coplanar waveguide with meshed and finite ground planes. WAMICON 2014, Tampa, FL, USA: IEEE; 2014, p. 1–3.
[8] Shih C-C, Burnette M, Staack D, Wang J, Tai BL. Effects of cold plasma treatment on interlayer bonding strength in FFF process. Addit Manuf 2019;25:104–11.
[9] Ferreira RTL, Amatte IC, Dutra TA, Bürger D. Experimental characterization and micrography of 3D printed PLA and PLA reinforced with short carbon fibers. Compos Part B Eng 2017;124:88–100.
[10] Pierson H, Celik E, Abbott A, Jarnette H, Gutierrez L, Johnson K, et al. Mechanical properties of printed epoxy-carbon fiber composites. Exp Mech 2019;59:843–57.
[11] van de Werken N, Tekinalp H, Khanbolouki P, Ozcan S, Williams A, Tehrani M. Additively manufactured carbon fiber-reinforced composites: State of the art and perspective. Addit Manuf 2020;31:100962–80.
[12] Hambali RH, Cheong KM, Azizan N. Analysis of the influence of chemical treatment to the strength and surface roughness of FDM. IOP Conf Ser Mater Sci Eng 2017;210:012063–72.
[13] Lavecchia F, Percoco G, Pei E, Galantucci L. Computer numerical controlled grinding and physical vapor deposition for fused deposition modelled workpieces. Adv Mater Sci Eng 2018;2018:1–7.
[14] Mireles J, Adame A, Espalin D, Medina F, Winker R, Hoppe T, et al. Analysis of sealing methods for FDM-fabricated Parts. 22nd Annu Int Solid Free Fabr Symp – Addit Manuf Conf SFF 2011, p. 185–96.
[15] Žigon J, Kariž M, Pavlič M. Surface finishing of 3D-printed polymers with selected coatings. Polymers 2020;12:2797–810.
[16] Dugbenoo E, Arif M, Wardle B, Kumar S. Enhanced bonding via additive manufacturing-enabled surface tailoring of 3D printed continuous-fiber composites. Adv Eng Mater 2018;20:1800691–9.
[17] Shahid M, Hashim SA. Effect of surface roughness on the strength of cleavage joints. Int J Adhes Adhes 2002;22:235–44.
[18] Xu Y, Unkovskiy A, Klaue F, Rupp F, Geis-Gerstorfer J, Spintzyk S. Compatibility of a silicone impression/adhesive system to FDM-printed tray materials–a laboratory peel-off study. Materials 2018;11:1905–21.
[19] Kariz M, Krapež Tomec D, Dahle S, Kuzman M, Sernek M, Zigon J. Effect of sanding and plasma treatment of 3D-printed parts on bonding to wood with PVAc adhesive. Polymers 2021;13:1211–26.
[20] Holmberg J, Wretland A, Berglund J, Beno T. Surface integrity after post processing of EDM processed Inconel 718 shaft. Int J Adv Manuf Technol 2018;95:2325–37.
[21] Orme M, Gschweitl M, Ferrari M, Madera I, Mouriaux F. Designing for additive manufacturing: lightweighting through topology optimization enables lunar spacecraft. J Mech Des 2017;139:100905–10.
[22] Chotiprayanakul P, Noda A. Preliminary study of epoxy coating process on basketry inlay with 3D printed model. IOP Conf Ser Mater Sci Eng 2019;639:012020–4.
[23] Belter JT, Dollar AM. Strengthening of 3D printed fused deposition manufactured parts using the fill compositing technique. PLOS ONE 2015;10:0122915–33.
[24] Saliu HR, Ishiaku US, Yakubu MK, Kolawole EG, Adefila SS, Bakar MBA, et al. The effect of epoxy concentration and fibre loading on the mechanical properties of ABS/epoxy-coated kenaf fibre composites. Open J Compos Mater 2015;05:41–8.
[25] LOCTITE® PC 7202™ Technical Data Sheet. Henkel; 2020. https://tdsna.henkel.com/americas/na/adhesives/hnauttds.nsf/web/39FA42E3365640158825718700000D97C/$File/PC%207202-EN.pdf (accessed February 27, 2022).
[26] 105 Epoxy Resin® / 205 Fast Hardener®. West System Technical Data Sheet. Bay-City, Michigan: West-Systems; 2014. https://www.westsystem.com/wp-content/uploads/105-205-Epoxy-Resin.pdf (accessed February 27, 2022).
[27] Technical Data Sheet Epoxy Resin PX439N. Hunts Rise, United Kingdom: Robnor Resins Ltd; 2009. http://www.farnell.com/datasheets/841920.pdf (accessed February 27, 2022).
[28] Yli-Opas P, Kattelus J, Ikäheimo A, Kittilä E, Vilenius V. Usage of consumer grade additive manufacturing of PLA for hybrid rockets. AIAA Propuls Energy Forum, 2019 American Institute of Aeronautics and Astronautics Inc. (AIAA).
[29] Sathishkumar N, Vincent B, Arunkumar N, Kumar KM, Sudharsan PL. Study of compressive behaviour on 3D printed ABS polymer lattice structures infilled with epoxy and polyester resins. IOP Conf Ser Mater Sci Eng 2020;923:012044–53.
[30] Zaldivar RJ, McLouth TD, Patel DN, Severino JV, Kim HI. Strengthening of plasma treated 3D printed ABS through epoxy infiltration. Prog Addit Manuf 2017;2:193–200.
[31] Epoxy. Fiberglass Supply. http://www.fiberglasssupply.com/product_catalog/epoxy/epoxy.html (accessed August 17, 2021).
[32] Impact-Resistant 3D Printer Filaments. McMaster-Carr. https://www.mcmaster.com/3d-printers-abs/ (accessed February 27, 2022).
[33] Bahramnia H, Semnani HM, Habibolahzadeh A, Abdoos H. Epoxy/polyurethane hybrid nanocomposite coatings reinforced with MWCNTs and SiO2 nanoparticles: processing, mechanical properties and wear behavior. Surf Coat Technol 2021;415:127121.
[34] Czél G, Jalalvand M, Wisnom MR. Hybrid specimens eliminating stress concentrations in tensile and compressive testing of unidirectional composites. Compos Part Appl Sci Manuf 2016;91:436–47.
[35] Gao H, Kaweesa D, Moore J, Meisel NA. Investigating the impact of acetone vapor smoothing on the strength and elongation of printed ABS parts. JOM 2016;69:580–85.
[36] Leite M, Varanda A, Silva A, Ribeiro A, Vaz MF. Water absorption and mechanical properties evaluation of surface modified ABS printing parts. Pro-AM 2016, Nanyang Technical University, Singapore: Pro-AM; 2016, p. 575-80.
[37] Kozior T, Mamun A, Trabelsi M, Sabantina L, Ehrmann A. Quality of the surface texture and mechanical properties of FDM printed samples after thermal and chemical treatment. J Mech Eng 2020;66:105–13.
[38] Jayanth N, Senthil P, Prakash C. Effect of chemical treatment on tensile strength and surface roughness of 3D-printed ABS using the FDM process. Virtual Phys Prototyp 2018;13:155–63.
[39] Singh R, Singh S, Singh IP, Fabbrocino F, Fraternali F. Investigation for surface finish improvement of FDM parts by vapor smoothing process. Compos B Eng 2017;111:228–34.
[40] Neff C, Trapuzzano M, Crane NB. Impact of vapor polishing on surface quality and mechanical properties of extruded ABS. Rapid Prototyp J 2018;24:501–8.
[41] Mu M, Ou C, Wang J, Liu Y. Surface modification of prototypes in fused filament fabrication using chemical vapour smoothing. Addit Manuf 2020;31:100972–82.
[42] Watanabe S, Kodama E, Sakakibara K, Sasaki S, Tsujii Y. Effect of surface texturing on the durability of concentrated polymer brushes. Tribol Int 2020;155:106668.
[43] Aziz R, Ul Haq MI, Raina A. Effect of surface texturing on friction behaviour of 3D printed polylactic acid (PLA). Polym Test 2020;85:106434–64.
[44] Kuijt-Evers LFM, Morel KPN, Eikelenberg NLW, Vink P. Application of the QFD as a design approach to ensure comfort in using hand tools: can the design team complete the house of quality appropriately? Appl Ergon 2009;40:519–26.
[45] Loring B, Lemieux E-A. User research improves laparoscopic instruments. Ergon Des 2010;18:18–23.
[46] Tawk C, Gao Y, Mutlu R, Alici G. Fully 3D printed monolithic soft gripper with high conformal grasping capability. 2019 IEEEASME Int. Conf. Adv. Intell. Mechatron. AIM, 2019, p. 1139–44.
[47] George M, Aroom KR, Hawes HG, Gill BS, Love J. 3D printed surgical instruments: the design and fabrication process. World J Surg 2017;41:314–19.
[48] Mashayekhi F, Bardon J, Berthé V, Perrin H, Westermann S, Addiego F. Fused filament fabrication of polymers and continuous fiber-reinforced polymer composites: advances in structure optimization and health monitoring. Polymers 2021;13:789–816.
[49] Ferrell WH, Arndt CM, TerMaath S. Tensile strength dependence of FFF fiber reinforced ABS on environmental conditioning. Mech Adv Mater Struct 2021;28:2163–76.
[50] Pineda AFE, Garcia FG, Simões AZ, Silva EL da. Mechanical properties, water absorption and adhesive properties of diepoxy aliphatic diluent-modified DGEBA/cycloaliphatic amine networks on 316L stainless steel. Int J Adhes Adhes 2016;68:205–11.
[51] Woo M, Piggott MR. Water absorption of resins and composites: IV.

water transport in fiber reinforced plastics. J Compos Technol Res 1988;10:20–24.

[52] Fortus® 250mc 3D Production System User Guide. Eden Prairie, MN: Stratasys, Inc.; 2016. https://ingenioer.au.dk/fileadmin/www.ase.au.dk/Filer/Laboratorier_og_vaerksteder/MakerLab/Fortus_250mc_User_Guide.pdf (accessed February 27, 2022).

[53] P430 ABSplus Model Cartridge / Fortus 250mc / Dimension Elite / 1200BS. GoEngineer Online Store. https://store.goengineer.com/products/p430-absplus-model-cartridge-black-56-cu-in (accessed February 27, 2022).

[54] MTS Criterion Series 40 Model 45. NDSU Research Equipment Inventory. http://researchtoolbox.ndsuresearchpark.com/inventory/196774 (accessed February 27, 2022).

[55] Portable Surface Roughness Tester Surftest SJ-210 Series. Aurora, IL: Mitutoyo America Corporation; 2021. https://www.mitutoyo.com/webfoo/wp-content/uploads/Surftest_SJ210.pdf (accessed February 27, 2022).

[56] 3 Flute-Standard Length-Single End Square-TiCN. HTC Tool-Cutter Manufacturing. http://www.htcmfg.com/index.php?route=product/product&path=7_1&product_id=496 (accessed February 27, 2022).

[57] Vagovský J, Buranský I, Görög A. Evaluation of measuring capability of the optical 3D scanner. Procedia Eng 2015;100:1198–206.

[58] ATOS Core | Portable 3D Scanner. Capture3D. https://www.capture3d.com/3d-metrology-solutions/3d-scanners/atos-core (accessed February 27, 2022).

[59] Dickin F, Pollard S, Adams G. Mapping and correcting the distortion of 3D structured light scanners. Precis Eng 2021;72:543–55.

[60] The LX Laser Extensometer Series. Eden Prairie, Minnesota: MTS; 2009. https://www.mts.com/-/media/materials/pdfs/brochures/mts-lx-laser-extensometer-brochure.pdf?as=1 (accessed February 27, 2022).

[61] Neff C, Elston E, Schrand A, Crane N. Adhesion testing of printed inks while varying the surface treatment of polymer substrates. J Adhes 2021;97:399–416.